Chinese Chemical Letters 37 (2026) 112434

Contents lists available at ScienceDirect

Chinese Chemical Letters

journal homepage: www.elsevier.com/locate/cclet

Tandem photochemical reduction-electrochemical oxidation process for extensive mineralization of refractory cyanuric acid in wastewater

Wenxiao Zheng, Jianyu Pan, Xin Luo, Huanxin Ma, Rundong Chen, Chunhua Feng*

The Key Lab of Pollution Control and Ecosystem Restoration in Industry Clusters, Ministry of Education, School of Environment and Energy, South China University of Technology, Guangzhou 510006, China

ARTICLE INFO

Article history:
Received 4 August 2025
Revised 22 November 2025
Accepted 18 January 2026
Available online 20 January 2026

Keywords:
UV/sulfite
Electrochemical oxidation
Tandem process
Cyanuric acid
Complete mineralization
Reaction mechanism

ABSTRACT

Cyanuric acid (CA), a stable triazine-based compound widely used in chlorinated disinfectants, has emerged as a recalcitrant contaminant frequently detected in aquatic environments. Due to its high chemical stability and electron-deficient structure, CA resists degradation by conventional oxidative processes. Here, a tandem UV/sulfite (SF)-based photochemical reduction-electrochemical oxidation (EO) process was developed to achieve complete mineralization of CA. Hydrated electrons generated in the UV/SF process efficiently induce triazine ring-opening, while EO further oxidizes the resulting intermediates. Density functional theory calculations and quenching experiments revealed that CA exhibits high activation barriers toward direct oxidation by $^{\bullet}OH$ and $SO_4^{\bullet-}$, explaining their limited reactivity. In contrast, direct electron transfer to the boron-doped diamond (BDD) anode dominates CA degradation in the EO process, albeit with sluggish kinetics due to the high oxidation potential. The tandem system effectively lowers the oxidative energy barrier via reductive fragmentation. Moreover, the UV/SF-EO process demonstrated reliable and effective performance in natural waters and industrial effluents. This study not only highlights the synergistic benefits of coupling reduction and oxidation for the treatment of persistent organic pollutants but also provides mechanistic insight into CA degradation pathways, offering a promising strategy for mitigating CA pollution in complex water environments.

© 2026 Published by Elsevier B.V. on behalf of Chinese Chemical Society and Institute of Materia Medica, Chinese Academy of Medical Sciences.

Since the global outbreak of COVID-19, frequent viral mutations have continued to disrupt public health systems and economic development, driving the widespread adoption of personal and environmental disinfection strategies. Among disinfectants, chlorinated cyanurates (Cl-CAs) are increasingly used as disinfectants in swimming pools and drinking water in various countries and regions [1–3]. Driven by global demand, the Cl-CAs market now exceeds US$ 196 million annually [4], with production in China alone rising by 14% in 2020 compared to pre-pandemic levels [5]. However, large volumes of cyanuric acid (CA) are generated both as a byproduct during Cl-CA manufacturing and as a residual compound during disinfection. CA levels in impacted water bodies often exceed the WHO guideline of 40 mg/L, with values >100 mg/L frequently reported in poorly managed or reused water [6,7]. It has also been detected in agricultural runoff, and industrial effluents [8,9]. Moreover, CA has been associated with nephrotoxic effects in humans and animals when co-exposed with melamine [10,11], particularly in children [12,13], raising increasing environmental and health concerns. In recognition of its persistence and uncertain ecological impacts, CA has been included in the European Commission list of emerging pollutants [14,15]. Therefore, it is crucial to effectively remove CA during water and wastewater treatment.

Structurally, CA features a highly stable triazine ring (a six-membered ring containing three nitrogen atoms), conferring exceptional resistance to oxidation [16,17]. As a result, CA is recalcitrant to degradation by conventional advanced oxidation processes (AOPs) [18–20], exhibiting various reactivity limitations. Previous studies have shown that UV/sulfite (UV/SF)-based advanced reduction processes (ARPs), which generate hydrated electrons (e_{aq}^-, $E = -2.9$ V *vs.* NHE) [21,22], are capable of cleaving the triazine ring [23,24]. However, they are ineffective at further degrading the resulting ring-opened intermediates, leading to substantial residual TOC and an increased risk of toxic byproduct accumulation. Recently, reduction-assisted oxidation strategies have gained increasing attention for the treatment of recalcitrant pollutants [25–29]. These approaches aim to first reduce parent molecules, thereby lowering the oxidation energy barrier, followed by oxidation-based mineralization of transformation intermediates [28,30]. The UV/SF-electrochemical oxidation (EO) tandem process is a representa-

* Corresponding author.
E-mail address: chfeng@scut.edu.cn (C. Feng).

https://doi.org/10.1016/j.cclet.2026.112434
1001-8417/© 2026 Published by Elsevier B.V. on behalf of Chinese Chemical Society and Institute of Materia Medica, Chinese Academy of Medical Sciences.

tive example that has achieved near-complete defluorination and mineralization of per- and polyfluoroalkyl substances (PFAS), a rare nonthermal technology capable of breaking strong C-F bonds [26,31]. Inspired by this success, we hypothesize that the UV/SF-EO tandem process could also overcome the degradation barriers of CA by integrating the strengths of reductive ring-opening and oxidative mineralization. Specifically, UV/SF pretreatment can effectively cleave the chemically inert triazine ring [23], while subsequent EO treatment enables the mineralization of the resulting ring-opening intermediates [26,29]. This combination helps to address the limitations of each individual process, specifically by overcoming the poor reactivity of CA toward EO and the inability of UV/SF to further degrade ring-opening intermediates, thereby offering a promising solution for the extensive mineralization of recalcitrant CA.

In this study, we systematically evaluate the UV/SF-EO tandem process for the complete degradation of CA, with a focus on elucidating the underlying synergistic mechanisms. CA removal efficiency was compared across different treatment strategies, while high-resolution mass spectrometry (HRMS) and computational toxicology were used to track transformation products and assess their toxicity. Dominant reactive species were identified via electron paramagnetic resonance (EPR), and density functional theory (DFT) calculations were conducted to explore reaction pathways at the molecular level. The reliability of this process was further validated in various real-water matrices and industrial wastewater scenarios. The details of experimental procedures and methods are shown in Texts S1-S4 (Supporting information).

The transformation behavior of CA under various treatment processes was comprehensively examined. CA exhibited strong resistance to degradation by either UV irradiation or sulfite alone (Fig. S1 in Supporting information). Complete transformation of CA was observed only in the UV/SF system, with nearly complete removal within 3 h (Fig. 1a). In the UV/SF system, UV light excites sulfite ions (SO_3^{2-}) to produce $SO_3^{\bullet-}$ and e_{aq}^-. Due to its strong reducing capability [22,32], e_{aq}^- attacks CA by cleaving the C–N bonds in the triazine ring, in agreement with previous observations [23,24]. However, the limited removal of TOC indicated the accumulation of a substantial amount of intermediate products. Even after extending the reaction time to 6 h, >70 % of TOC remained in solution. Although the UV/SF system has been widely applied for dehalogenation of halogenated compounds or the detoxification of heavy metals (*e.g.*, Sb(V)) [25,32,33], it is inherently limited in its ability to achieve effective mineralization of recalcitrant organic pollutants [34].

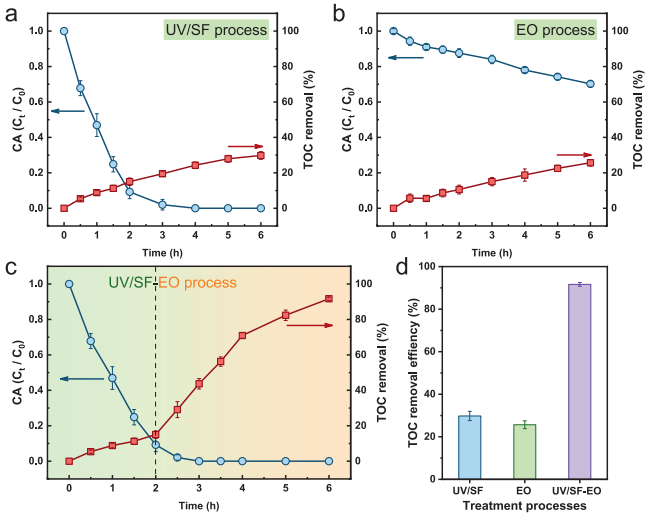


Fig. 1. Time courses of CA concentration and TOC removal in (a) UV/SF, (b) EO, and (c) UV/SF-EO processes. (d) Comparison of TOC removal efficiencies among different treatment processes. Reaction conditions: $[CA]_0 = 0.4$ mmol/L, initial pH 10, $[SF]_0 = 30$ mmol/L for UV/SF process, and current density = 20 mA/cm^2 for EO process. Note: In the UV/SF-EO process, the time segment before the dashed line represents the UV/SF stage, while the segment after corresponds to the EO stage.

To assess the performance of EO for CA treatment, both an active Ti/RuO_2-IrO_2 anode and typical inert anodes (Ti/PbO_2 and BDD) were evaluated. Only limited CA degradation was observed, occurring exclusively with inert anodes (Fig. S2 in Supporting information). Even with the BDD anode that is considered the benchmark in EO applications, <30 % of CA was degraded after 6 h of continuous electrolysis (Fig. 1b). Despite the limited CA degradation, TOC removal closely tracked CA degradation, contrasting with the UV/SF system where TOC removal lagged significantly. This suggests that CA ring-opening products are more amenable to oxidation in the EO system, while the degradation of CA itself constitutes the rate-limiting step for TOC removal. Thus, although EO faces challenges in degrading CA, it exhibits a clear advantage over UV/SF in facilitating TOC reduction.

Additional experiments were conducted using the integrated UV/SF-EO process to examine its effectiveness in CA transformation and mineralization. During the UV/SF stage, CA was almost completely removed within 2 h, followed by a slow decline in TOC. At this critical point, UV/SF treatment was halted, and EO treatment was initiated. Although residual SF might have remained in the solution, its concentration was rapidly depleted during the EO process and did not interfere with the subsequent oxidation of degradation intermediates (Fig. S3 in Supporting information). As the EO process proceeded, the TOC concentration decreased rapidly, achieving over 90 % removal within a total operating time of 6 h (Fig. 1c). Remarkably, the TOC removal rate in the tandem process significantly exceeded those of the individual UV/SF and EO process, and even the sum of their separate contributions (Fig. 1d). The *pseudo*-first-order rate constant for TOC removal in the UV/SF-EO process (0.4309 h^{-1}) was markedly higher than that of UV/SF (0.0648 h^{-1}) and EO (0.0467 h^{-1}) alone (Fig. S4 in Supporting information). In addition, since the cleavage of CA involves deamination reactions, the UV/SF process mainly resulted in the release of NH_4^+-N (Fig. S5 in Supporting information). During the subsequent EO stage, the majority of the NH_4^+-N was directly oxidized to N_2, with only minor amounts of NO_2^--N and NO_3^--N detected as over-oxidation products. These over-oxidation products were further reduced at the cathode to N_2, resulting in effective overall nitrogen removal. The specific energy consumption (SEC) for mineralization removed (kwh/g TOC) was estimated based on our experimental parameters. As shown in Fig. S6 (Supporting information), the tandem UV/SF-EO process achieved a markedly lower SEC of 6.2 kWh/g TOC compared with 12.3 kWh/g TOC for UV/SF alone and 25.6 kWh/g TOC for EO alone. This result indicates the energy advantage of the combined process in achieving extensive mineralization relative to either single treatment. These results confirm that the integrated UV/SF-EO process maximizes the complementary advantages of both individual systems, demonstrating superior performance in the complete mineralization of CA.

Short-chain carboxylic acids formed during CA degradation were quantified throughout the reaction. Fig. 2a shows that the UV/SF process led to the formation of formic and acetic acids. Although CA lacks carbon chains in its molecular structure, the generation of carbon-centered radicals under strong reductive conditions, followed by rearrangement reactions, likely accounts for acetic acid formation [35]. These low-molecular-weight acids were degraded during EO treatment, demonstrating the enhanced mineralization capability of the EO process. In addition, a series of ring-opening and chain-shortening intermediates were identified *via* Orbitrap-HRMS. The detection of 1-carboxybiuret (**P1**) and 2,4-diimidotricarbonic acid (**P2**) confirmed triazine ring cleavage in the

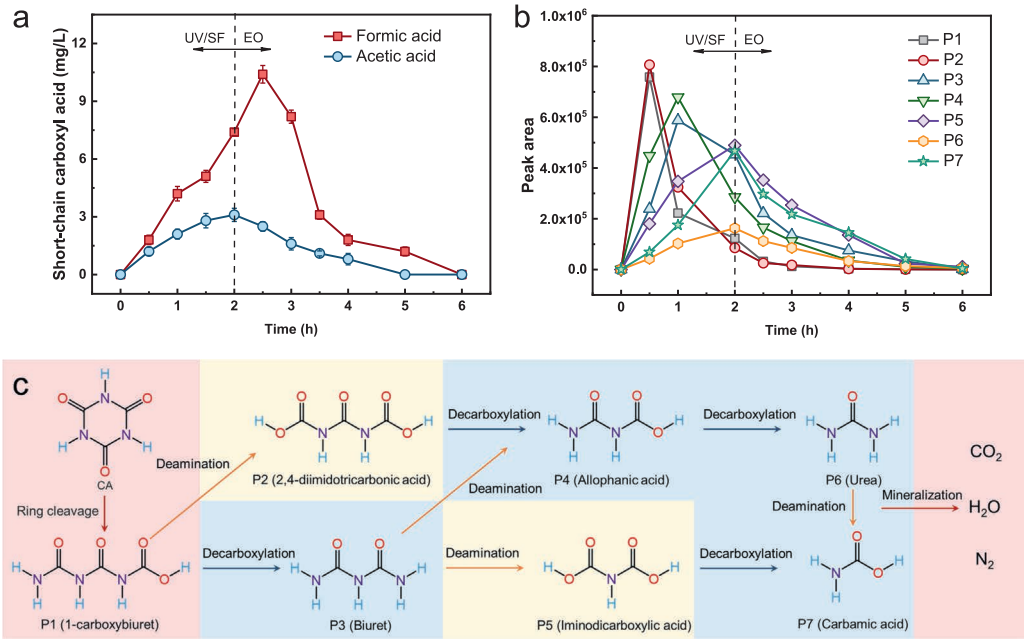


Fig. 2. (a) Time courses of carboxylic acid concentrations in the UV/SF-EO process. (b) Time courses of the peak areas of degradation intermediates identified by HRMS. (c) Proposed degradation pathways of CA in the UV/SF-EO process. Reaction conditions: $[CA]_0 = 0.4$ mmol/L, initial pH 10, $[SF]_0 = 30$ mmol/L for UV/SF, and current density = 20 mA/cm^2 for EO.

UV/SF step. Other intermediates, including biuret (**P3**), allophanic acid (**P4**), iminodicarboxylic acid (**P5**), urea (**P6**), and carbamic acid (**P7**), were also detected (Table S1 in Supporting information), indicating pathways involving deamination and decarboxylation. HRMS peak areas (Fig. 2b) showed substantial accumulation of these intermediates during UV/SF treatment, suggesting their limited reactivity toward further reductive degradation. Given the potential toxicity of these intermediates, developmental toxicity was assessed using the U.S. EPA's Toxicity Estimation Software Tool, based on quantitative structure–activity relationship (QSAR) models [25,36]. As illustrated in Fig. S7, CA itself was predicted to be developmentally toxic. It is noticeable that all intermediates (except for the initial ring-opening products **P1** and **P2**) exhibited higher predicted toxicity than CA and were also classified as toxicants. Although the QSAR-based predictions are preliminary, these findings underscore the importance of achieving complete mineralization to eliminate potentially harmful intermediates. During EO treatment, nearly all identified intermediates were effectively removed, implying the strong non-selective oxidation capacity of the EO process.

A degradation pathway for CA was proposed, as depicted in Fig. 2c. In the UV/SF process, the triazine ring of CA is initially cleaved to generate intermediate **P1**, which can undergo deamination to form **P2** or decarboxylation to yield P3. Subsequent deamination and decarboxylation steps result in the formation of additional intermediates, including **P4**, **P5**, **P6**, and **P7**. Upon transitioning to the EO stage, these accumulated intermediates are effectively mineralized, as indicated by the >90 % TOC removal efficiency.

EPR spectroscopy was used to identify the reactive species responsible for CA conversion and intermediate degradation in the UV/SF and EO processes. In the UV/SF system, e_{aq}^- was generated *via* sulfite photolysis under UV irradiation [22]. TEMPO, a selective e_{aq}^- probe, exhibits a characteristic triplet EPR signal that diminishes upon reduction to EPR-silent TEMP [37]. Fig. 3a shows that the EPR signal of TEMPO remained unchanged when UV or sulfite was applied alone but significantly decreased under combined UV/SF conditions, confirming e_{aq}^- formation. Time-resolved monitoring of TEMPO decay (Fig. 3b) delivered a steady decay rate, consistent with constant e_{aq}^- generation likely due to sustained sulfite consumption (Fig. S8 in Supporting information).

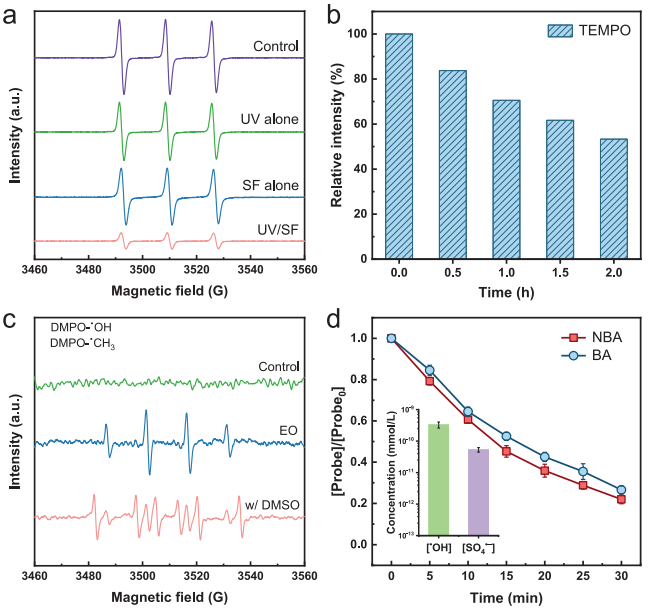


Fig. 3. (a) TEMPO-probed EPR spectra of e_{aq}^- in different systems. (b) Time-resolved TEMPO decay in the UV/SF process. (c) DMPO spin-trapping EPR spectra in different systems. (d) Quantification of •OH and $SO_4^{\bullet-}$ using selective probe compounds. Reaction conditions: $[CA]_0 = 0.4$ mmol/L, initial pH 10, $[SF]_0 = 30$ mmol/L for UV/SF, current density = 20 mA/cm^2 for EO, [TEMPO] = 0.5 mmol/L for (a), 10 mmol/L for (b), [DMPO] = 100 mmol/L, and $[Probe]_0 = 20$ μmol/L.

In the EO process at 20 mA/cm^2, the anodic potential (~3.41 V *vs.* RHE) (Fig. S9 in Supporting information) exceeded the thresholds for formation of both •OH and $SO_4^{\bullet-}$, which can be detected using DMPO as a spin trap [38]. Fig. 3c depicts that only the DMPO-•OH adduct was observed. It should be noted that the DMPO-$SO_4^{\bullet-}$ adduct can rapidly convert to DMPO-•OH *via* substitution with water or OH^- (Fig. S10 in Supporting information)

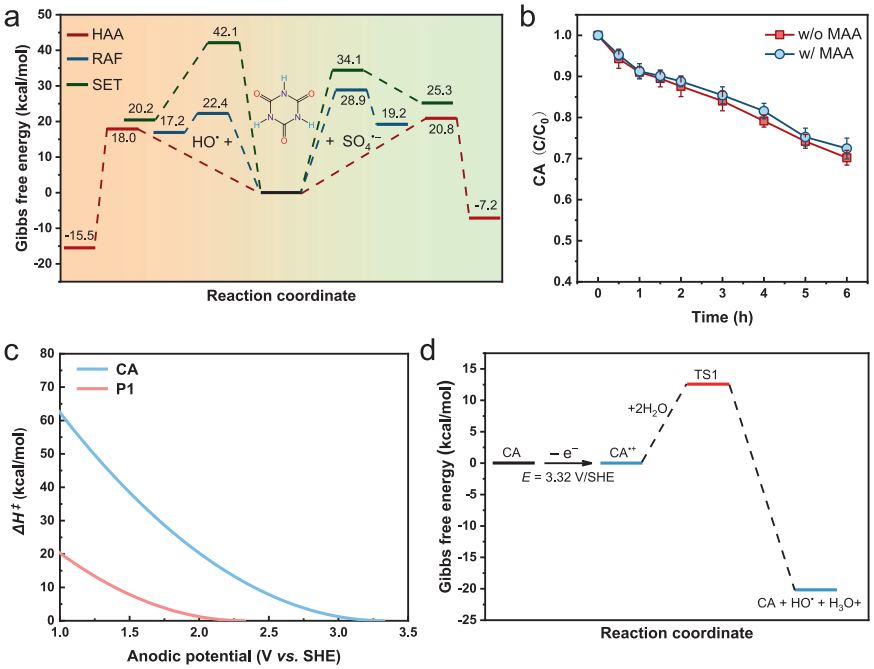


Fig. 4. (a) Schematic free energy profiles of the initial elementary reaction of CA oxidation by •OH and $SO_4^{\bullet-}$ *via* different pathways. (b) CA degradation trends in the EO process with and without MAA. (c) Activation enthalpy ($\Delta H\ddagger$) for the target molecule to lose one electron as a function of anodic potential *versus* standard hydrogen electrode (SHE). (d) DFT-calculated energy diagram for the electrochemical oxidation of CA at 3.32 V *vs.* SHE, with TS denoting the transition state. Reaction conditions: $[CA]_0 = 0.4$ mmol/L, initial pH 10, current density = 20 mA/cm^2 for EO, and [MAA] = 10 mmol/L.

[39,40]. To differentiate •OH and $SO_4^{\bullet-}$, DMSO was added as a scavenger. Since •OH reacts with DMSO to yield $^{\bullet}CH_3$, the presence of DMPO-$^{\bullet}CH_3$ indicates •OH generation [21,39]. The EPR spectrum similarly showed incomplete suppression of DMPO-•OH by DMSO, supporting the coexistence of $SO_4^{\bullet-}$. To quantify radical concentrations, 4-nitrobenzoic acid (NBA) and benzoic acid (BA) were used as selective probes for •OH and $SO_4^{\bullet-}$, respectively [41]. Kinetic analysis (Fig. S11 in Supporting information) yielded steady-state concentrations of 3.31×10^{-10} mmol/L for •OH and 5.34×10^{-11} mmol/L for $SO_4^{\bullet-}$ (Fig. 3d).

A particularly noticeable observation is that despite the generation of highly reactive •OH and $SO_4^{\bullet-}$ species by the BDD anode, <30 % of CA was degraded after 4 h of electrolysis. In contrast, complete transformation occurred within 3 h in the UV/SF process. This apparent discrepancy prompts investigation into the actual contribution of •OH and $SO_4^{\bullet-}$ to CA degradation. To assess their roles, UV/H_2O_2 and UV/PDS systems were applied to selectively generate •OH and $SO_4^{\bullet-}$, respectively. Neither system achieved measurable CA degradation (Fig. S12 in Supporting information), suggesting these radicals have negligible impact on its direct transformation. In addition, EO treatments using Na_2SO_4 (generating both •OH and $SO_4^{\bullet-}$) and $NaClO_4$ (generating only •OH) showed comparable degradation profiles (Fig. S13 in Supporting information) [26], further ruling out the involvement of specific reactive species. This resistance can be attributed to the oxidation-resistant nature of the carbon atoms in CA, which are in a high oxidation state (+IV), similar to that in CO_2 [42].

DFT calculations were conducted to elucidate the limited reactivity of •OH and $SO_4^{\bullet-}$ toward CA oxidation. The molecular structure of CA comprises C–N, C=O, and N–H bonds (Fig. S14a in Supporting information). Among these, only the N–H bond shows a moderate bond dissociation energy (Fig. S14b in Supporting information), indicating that hydrogen atom abstraction (HAA) reactions are limited to this specific site. Regarding the radical adduct formation (RAF) pathway, the Fukui function (f^-) analysis revealed that the C1 positions exhibit the highest electrophilic susceptibility (Fig. S14c in Supporting information), suggesting that they are preferred sites for radical attack *via* π addition [43]. Molecular orbital analysis further indicated that electron loss is most likely to occur at the N atoms within the triazine ring, due to their lone pairs and strong contribution to the delocalized π-system [44], favoring the single electron transfer (SET) pathway. The optimized structures of all investigated pathways are shown in Fig. S15 (Supporting information). Fig. 4a shows that all reactions exhibit activation energies ($\Delta G\ddagger$) exceeding 18 kcal/mol, indicating that CA oxidation by •OH and $SO_4^{\bullet-}$ is kinetically unfavorable, consistent with the limited degradation observed experimentally.

Based on these findings, we propose that CA degradation during the EO process is primarily driven by direct electron transfer (DET) from CA to the BDD electrode, rather than by radical-mediated reactions. To evaluate this mechanism, β-methallyl alcohol (MAA), a known scavenger of surface-bound oxidants due to its reactive π-orbitals and allylic carbon [45], was introduced. As illustrated in Fig. 4b, MAA addition had only a minor effect on CA degradation, likely due to competitive adsorption at the electrode surface rather than effective scavenging of reactive species. This supports the conclusion that DET is the dominant pathway. Despite enabling DET-driven CA oxidation, the EO process suffers from slow kinetics. DFT calculations (Fig. 4c) indicated that DET from CA occurs only at high anodic potentials (~3.32 V *vs.* SHE), which exceeds the onset potentials for •OH (2.7 V) and $SO_4^{\bullet-}$ (3.1 V) generation [46,47]. This high potential requirement accounts for the sluggish reaction kinetics. Importantly, once oxidized to the CA$^{\bullet+}$ radical, CA may spontaneously revert to its parent form in aqueous solution, as suggested by a favorable ΔG (−20.2 kcal/mol) and moderate $\Delta G\ddagger$ (Fig. 4d). These results reaffirm the inherent resistance of CA to oxidation and explain its poor removal efficiency in conventional oxidative systems.

It is highlighted in Fig. 1a that e_{aq}^- generated from the UV/SF system effectively reduced CA. Monochloroacetic acid (MCAA), a well-established probe for e_{aq}^- in UV/SF systems (Fig. S16 in Supporting information) [48,49], was ued to determine the second-

order rate constant between e_{aq}^- and CA via a competition kinetics approach. A relatively high second-order rate constant (ke_{aq}^-, CA = 1.21×10^8 L mol^{-1} s^{-1}) was obtained (Fig. S17 in Supporting information), suggesting the appreciable reactivity of CA toward e_{aq}^-. Moreover, the ring-opening product **P1**, formed upon e_{aq}^- reduction of CA, exhibited increased susceptibility to anodic oxidation, requiring lower anodic potentials than CA, which supports the observation that TOC removal is rate-limited by the initial degradation of CA (Fig. 1b). Therefore, the pre-reduction of CA in UV/SF is a critical step in enabling its total degradation during subsequent EO treatment. These results provide valuable molecular-level insights into the limited reactivity of CA in EO process, and underscore the synergistic advantage of integrated UV/SF and EO for the complete mineralization of recalcitrant CA.

Given the widespread detection of CA in aquatic environments, it is essential to evaluate the performance of the UV/SF-EO process under realistic water conditions. Natural waters typically contain numerous coexisting constituents, including dissolved organic matter and inorganic ions, which may interfere with advanced radical-mediated processes [50,51]. To assess the matrix tolerance of the tandem system, tap water and surface water from the Zhujiang River were used as representative real-water matrices, with the main water quality parameters summarized in Tables S2 and S3 (Supporting information). Fig. S18 (Supporting information) shows that rapid transformation of CA was achieved in both matrices *via* the UV/SF process, accompanied by a moderate decrease in TOC (Fig. 5a). Subsequent EO treatment led to substantial TOC removal, indicating that CA and its intermediates were further mineralized to CO_2. Despite differences in ionic composition and background organic content, the degradation kinetics of CA and the extent of TOC removal in tap water and surface water were comparable to those observed in DI water. These results demonstrate that the UV/SF-EO process exhibits a high degree of robustness and tolerance for the treatment of CA in complex aqueous systems.

Point source control remains one of the most effective strategies for mitigating environmental pollution. Efficient treatment of industrial effluents containing CA is therefore essential for minimizing its environmental burden. To assess the practical applicability of the tandem process, a real wastewater sample was collected from the effluent of a Cl-CAs manufacturing facility. The primary water quality characteristics of this industrial effluent are listed in Table S4 (Supporting information), including a CA concentration of 0.48 mmol/L, a TOC concentration of 21.5 mg/L, and a high load of inorganic constituents. These conditions present considerable challenges for conventional treatment approaches. In agreement with results obtained from synthetic wastewater, both standalone UV/SF and EO processes exhibited limited performance in this complex matrix. While the UV/SF process enabled partial CA transformation (Fig. S19 in Supporting information), it yielded minimal TOC reduction, and the EO process alone was ineffective in degrading CA (Fig. 5b). Remarkably, the UV/SF-EO process retained its efficacy under these harsh conditions. Following 3 h of UV/SF pretreatment, an additional 5 h of EO treatment resulted in over 90 % TOC removal. Meanwhile, inorganic nitrogen species generated during CA degradation were also effectively removed during the EO stage (Fig. S20 in Supporting information). In addition, during five consecutive cycles with a cumulative operation time of 40 h, the UV/SF-EO process consistently maintained >90 % TOC removal (Fig. 5c) without any noticeable loss of mineralization efficiency.

In summary, we propose the UV/SF-EO tandem process that synergistically integrates reductive ring cleavage with subsequent oxidative mineralization. In this strategy, the UV/SF process rapidly generates e_{aq}^- to cleave the triazine ring structure, and thereby lowering the energy barrier for oxidation. Strong oxidants including $^{\bullet}OH$ and $SO_4^{\bullet-}$ are ineffective due to high activation energies ($\Delta G‡ > 18$ kcal/mol); although CA can be degraded *via* DET during EO, the process is kinetically limited by the high anodic potential required (3.32 V *vs.* SHE). In contrast, the ring-opening intermediates are more susceptible to oxidation, achieving near-complete TOC removal in the subsequent EO stage. This approach was successfully validated across a range of matrices, including synthetic wastewater, tap water, surface water, and actual industrial effluents. Overall, the UV/SF-EO tandem process represents a promising solution for the advanced treatment of emerging recalcitrant micropollutants by coupling energy-barrier-lowering reduction with efficient oxidative mineralization.

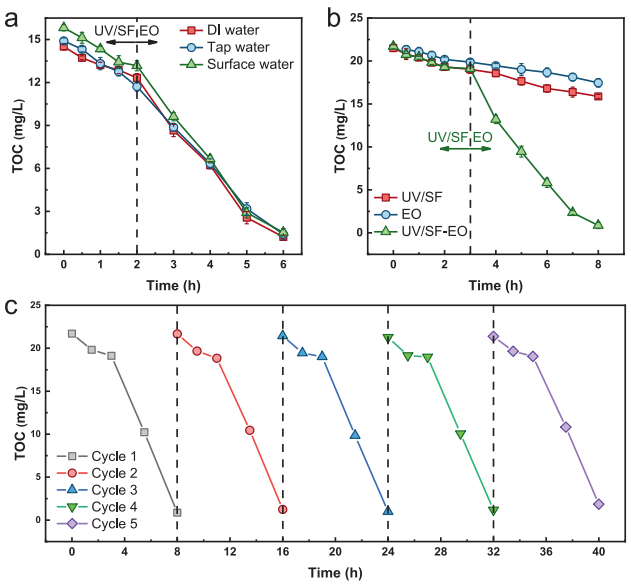


Fig. 5. (a) Time-dependent TOC removal during UV/SF-EO treatment of CA in different water matrices. (b) Comparison of TOC removal profiles for various treatment processes applied to real wastewater containing CA. (c) UV/SF-EO treatment of real wastewater containing CA operated over five consecutive cycles. Note: In each cycle, the first 3 h corresponded to the UV/SF process and the subsequent 5 h to the EO process. Reaction conditions: $[CA]_0 = 0.4$ mmol/L for (a), initial pH 10, $[SF]_0 = 30$ mmol/L for UV/SF, and current density = 20 mA/cm^2 for EO.

CRediT authorship contribution statement

Wenxiao Zheng: Writing – original draft, Investigation, Funding acquisition, Formal analysis, Data curation, Conceptualization. **Jianyu Pan:** Validation, Investigation, Data curation. **Xin Luo:** Validation, Investigation, Formal analysis. **Huanxin Ma:** Investigation, Formal analysis. **Rundong Chen:** Validation, Investigation. **Chunhua Feng:** Writing – review & editing, Supervision, Methodology, Funding acquisition, Conceptualization.

Declaration of competing interest

The authors declare that they have no known competing financial interests or personal relationships that could have appeared to influence the work reported in this paper.

Acknowledgments

This research was funded by the National Natural Science Foundation of China (Nos. 42407315 and U21A2034), the Guangdong Special Support Plan for Innovation Teams (No. 2019BT02L218), the Postdoctoral Fellowship Program of CPSF (No. GZB20240231), and the China Postdoctoral Science Foundation (Nos. 2024M760961 and 2025T18039).

Supplementary materials

Supplementary material associated with this article can be found, in the online version, at doi:10.1016/j.cclet.2026.112434.

References

[1] D.G. Wahman, J. Am. Water Work Assoc. 110 (2018) E1–E15.
[2] J. Zhao, C. Shang, R. Yin, Environ. Sci. Technol. 57 (2023) 18867–18876.
[3] I.M. Oliveira, I.B. Gomes, L.C. Simões, M. Simões, Sci. Total Environ. 811 (2022) 152355.
[4] W. Huang, Y. Li, F. Wang, et al., Water Res. 247 (2023) 120787.
[5] L. Zhao, Y. Lu, H. Zhu, et al., Environ. Int. 165 (2022) 107299.
[6] WHO, Guidelines for safe recreational water environments, 2006.
[7] WHO, Guidelines for drinking-water quality, 2017.
[8] J. Wang, Z. Hao, F. Shi, et al., Environ. Sci. Technol. 52 (2018) 5662–5670.
[9] H. Zhu, K. Kannan, Environ. Pollut. 258 (2020) 113743.
[10] R.P. Dalal, D.S. Goldfarb, Nat. Rev. Nephrol. 7 (2011) 267–274.
[11] B.G. Hammond, S.J. Barbee, T. Inoue, et al., Environ. Health Perspect. 69 (1986) 287–292.
[12] H.C. Hodge, B.J. Panner, W.L. Downs, E.A. Maynard, Toxicol. Appl. Pharmacol. 7 (1965) 667–674.
[13] N. Guan, Q. Fan, J. Ding, et al., New Engl. J. Med. 360 (2009) 1067–1074.
[14] K. Abdullahi, A. Elreedy, M. Fujii, M.G. Ibrahim, A. Tawfik, J. Adv. Res. 24 (2020) 211–222.
[15] I.J. Neuwald, D. Hübner, H.L. Wiegand, et al., Environ. Sci. Technol. 56 (2022) 10857–10867.
[16] B. Niu, J. Cai, W. Song, G. Zhao, Water Res. 205 (2021) 117663.
[17] A. Hiskia, M. Ecke, A. Troupis, et al., Environ. Sci. Technol. 35 (2001) 2358–2364.
[18] Y.H. Chuang, H.J. Shi, Water Res. 211 (2022) 118075.
[19] N. Watanabe, S. Horikoshi, H. Hidaka, N. Serpone, J. Photoch. Photobio. A 174 (2005) 229–238.
[20] S. Nélieu, L. Kerhoas, J. Einhorn, Environ. Sci. Technol. 34 (2000) 430–437.
[21] Y. Zhao, C. Zhang, L. Chu, et al., Water Res. 225 (2022) 119212.
[22] S. Zhang, H. Zheng, P.G. Tratnyek, Nat. Water 1 (2023) 666–681.
[23] X. Luo, W. Zheng, Q. Li, et al., Environ. Sci. Technol. 59 (2025) 5327–5336.
[24] Y. Tian, W. Shen, F. Jia, Z. Ai, L. Zhang, Chem. Eng. J. 330 (2017) 1075–1081.
[25] G. Song, R. Liang, J. He, et al., Appl. Catal. B: Environ. Energy 370 (2025) 125161.
[26] Y. Guan, Z. Liu, N. Yang, et al., Nat. Water 2 (2024) 443–452.
[27] J. Zhang, G. Zhang, H. Lan, et al., Environ. Sci. Technol. 57 (2023) 12117–12126.
[28] J. Zhang, Q. Ji, H. Lan, et al., Environ. Sci. Technol. 53 (2019) 14586–14594.
[29] G. Zhang, Y. Li, C. Zhao, et al., Nat. Nanotechnol. 19 (2024) 1130–1140.
[30] J. Zhang, G. Zhang, H. Lan, J. Qu, H. Liu, Environ. Sci. Technol. 55 (2021) 3296–3304.
[31] A. Alinezhad, H. Shao, K. Litvanova, et al., Environ. Sci. Technol. 57 (2023) 8796–8807.
[32] Z. Liu, Z. Chen, J. Gao, et al., Environ. Sci. Technol. 56 (2022) 3699–3709.
[33] F. Zhu, X. Zhang, X. Peng, et al., Environ. Sci. Technol. 59 (2025) 924–934.
[34] M.J. Bentel, Y. Yu, L. Xu, et al., Environ. Sci. Technol. 53 (2019) 3718–3728.
[35] Z. Liu, L.F. Wu, C.L. Kufner, et al., Nat. Chem. 13 (2021) 1126–1132.
[36] F. Wang, S.S. Liu, Z. Feng, et al., J. Hazard. Mater. 440 (2022) 129723.
[37] L. Chen, J. Duan, P. Du, et al., Water Res. 221 (2022) 118747.
[38] J.V. Macpherson, Phys. Chem. Chem. Phys. 17 (2015) 2935–2949.
[39] H.Y. Gao, C.H. Huang, L. Mao, et al., Environ. Sci. Technol. 54 (2020) 14046–14056.
[40] Y.H. Guan, J. Ma, X.C. Li, J.Y. Fang, L.W. Chen, Environ. Sci. Technol. 45 (2011) 9308–9314.
[41] P. Li, D. Xu, Y. Gao, et al., Water Res. 266 (2024) 122357.
[42] T.A. Tetzlaff, W.S. Jenks, Org. Lett. 1 (1999) 463–466.
[43] W. Zheng, X. Luo, H. Fu, et al., Environ. Sci. Technol. 58 (2024) 12212–12224.
[44] H. Zhang, C. Xie, L. Chen, et al., Water Res. 229 (2023) 119392.
[45] W. Lai, X. Yang, Z. Hua, et al., Water Res. 271 (2025) 122984.
[46] Y. Liu, X. Fan, X. Quan, et al., Environ. Sci. Technol. 53 (2019) 5195–5201.
[47] C. Kuang, G. Zeng, Y. Zhou, et al., Water Res. 229 (2023) 119464.
[48] B.D. Fennell, D. Fowler, S.P. Mezyk, G. McKay, Environ. Sci. Technol. 57 (2023) 7634–7643.
[49] B.D. Fennell, A. Odorisio, G. McKay, Environ. Sci. Technol. 56 (2022) 10329–10338.
[50] L. Cao, Z. Wang, Y. Cheng, et al., Environ. Sci. Technol. 57 (2023) 17629–17639.
[51] B.C. Hodges, E.L. Cates, J.H. Kim, Nat. Nanotechnol. 13 (2018) 642–650.